7 Charge Exchange Emission from H-like C and O Colliding on H_2O

Charge exchange emission in astrophysical environments is characterized by strong forbidden lines, and the relative strengths of the forbidden, resonance and intercombination lines following charge exchange are distinctly different from those due to other emission mechanisms (Kharchenko and Dalgarno, 2001). This has recently been demonstrated by Mars observations with XMM-*Newton* (Dennerl et al., 2006), which do resolve the OVII forbidden, resonance and intercombination lines. Using the relative strength of these lines, the observers were able to distinguish between fluorescence emission from the planetary disc and a CXE dominated halo due to solar wind interactions with the outer atmosphere.

The analysis of the Mars observations was based on the assumption that charge exchange populates the triplet and singlet states according to a statistical distribution, with a ratio of 3:1. Interestingly, no direct measurements or simulations of the collision systems of interest are available to support this assumption. The long lifetimes of the metastable states of solar wind ions make it very difficult to measure the resulting emission directly in a laboratory experiment. For example, the 2^3S state has a lifetime of 20 ms in CV, and 1 ms in OVII (Porquet and Dubau, 2000; Porquet et al., 2001). At typical solar wind velocities of 500 km s^{-1}, the ions cover a distance of 11 and 0.5 km, respectively.

Beiersdorfer et al. (2003) measured CXE spectra by trapping ions typical for the solar wind, and then injecting a target gas into the trap. The forbidden lines of He-like C, N and O were observed, but the experiment did not allow for direct measurement of the triplet-to-singlet (TS) ratio because of the mixing of the subshells induced by the large magnetic field used to trap the ions.

Suraud et al. (1991) investigated collisions between C^{5+} and H_2 by means of Far-UV Photon Emission Spectroscopy, which allowed for the direct measurement of some specific triplet and singlet emission cross sections. They measured a near to statistical TS population ratio of $\sigma_T/\sigma_S = 3.7$ at a collision energy of 4.3 keV/amu, which is close to the

statistical TS ratio. However, experiments with lower charged ions (O^{3+}, N^{4+}) and H and H_2 showed that at collision energies below 1 keV/amu, the TS-ratio changes significantly with decreasing collision energy (Beijers et al., 1996; Bliek et al., 1998). These findings are confirmed by theoretical simulations (Wang et al., 2002; Stancil et al., 1997). Preliminary theoretical results suggested a strong velocity dependence of the OVII triplet/singlet ratio for electron capture from helium (Krasnopolsky et al., 2004). Such an effect will have important consequences for the interpretation of CXE spectra if it also occurs with other collision targets, such as H_2O for comets.

Here, we present the first direct measurements of the velocity dependence of the ratio between capture into specific triplet- and singlet states following single electron capture (SEC) by H-like carbon and oxygen ions colliding with water molecules. These reactions can be summarized as:

$$A^{q+}(1s) + H_2O \rightarrow A^{(q-1)+}(1sn'\ell') + (H_2O)^+ \tag{7.1}$$

$$\rightarrow A^{(q-1)+}(1sn\ell) + (H_2O)^+ + h\nu \tag{7.2}$$

where the incoming projectile A^{q+} (C^{5+} or O^{7+}) captures one electron into an excited state $1sn'\ell'$, which subsequently decays to a lower lying state by emitting a photon.

The experiments are carried out in the energy range between $0.3-20q$ keV by means of photon emission spectroscopy, i.e., by detecting the extreme-ultraviolet photons emitted during the ions' relaxation (Chapter 4). The experiment therefore yields direct measurements of various EUV emission cross sections, from which by means of a spectroscopic analysis population cross sections are derived.

7.1 Atomic Structure of He-like ions

Because decay schemes work as a funnel, the lowest transitions ($n = 2 \rightarrow 1$) are the strongest emission lines in astrophysical CXE spectra. For helium-like ions, these are the forbidden line z (1^1S_0–2^3S_1), the intercombination lines y, x (1^1S_0–$2^3P_{1,2}$), and the resonance line w (1^1S_0–2^1P_1), see Fig. 7.1. For X-ray plasma diagnostics, two different ratios between these lines are used:

$$R = \frac{z}{x+y} \tag{7.3}$$

$$G = \frac{z+x+y}{w} \tag{7.4}$$

In electron collision dominated plasmas, the ratio R is sensitive to electron densities, and the ratio G to electron temperatures (Gabriel and Jordan, 1969). In the case of CXE, the G and R ratios solely depend on the initial $n\ell$-distribution and on the branching ratios of the ionic system of interest, and hence on the collision velocity and the electronic structure of the two colliding particles.

The apparent branching ratios for the decay of the 2^3P state are determined by weighting theoretical transition rates (Porquet and Dubau, 2000; Porquet et al., 2001) by an as-

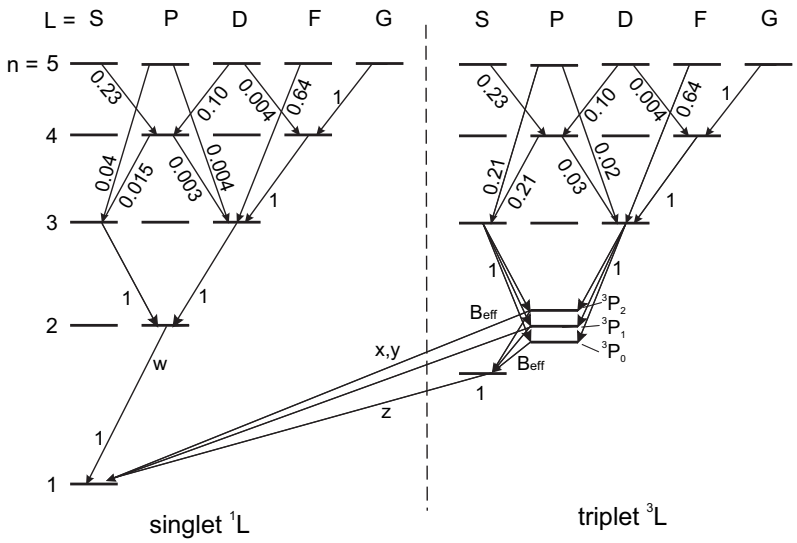

Figure 7.1: *Part of the decay scheme of a helium-like ion.*

Table 7.1: *Apparent effective branching ratios, B_{eff}, for the decay of the 2^3P state of He-like carbon and oxygen ions.*

transition	CV	OVII
1^1S_0–$2^3P_{1,2}$	0.11	0.30
2^3S_1–$2^3P_{0,1,2}$	0.89	0.70

sumed statistical population of the triplet P-term:

$$B_{eff} = \sum_{j=0}^{2} \frac{(2j+1)}{(2L+1)(2S+1)} \cdot \mathrm{B}_j \tag{7.5}$$

The resulting effective branching ratios are given in Table 7.1.

The ratio G is not equal to the overall triplet-to-singlet ratio, because in the singlet system the np-states decay to the ground state directly. G thus depends both on the triplet to singlet ratio, and on the initial distribution over the $n\ell$ states.

7.2 Analysis

7.2.1 C^{5+}

Charge exchange spectra following C^{5+}+H_2O collisions are complex and contain many emission lines. Equipped with a 1200 grooves/mm grating, our EUV spectrometer has a

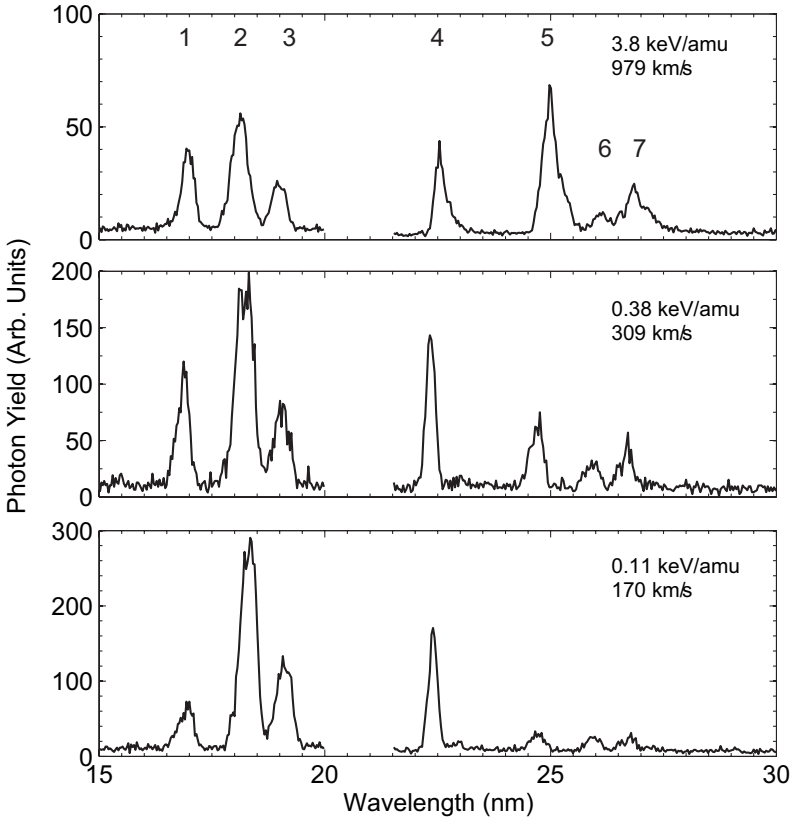

Figure 7.2: *Charge exchange spectra for collisions between C^{5+} and H_2O, at different velocities. The spectra are all on the same scale, i.e. corrected for the inlet pressure and integration time. The numbers above the figure refer to Table 7.4. The spectra are not corrected for the wavelength dependent sensitivity of the detection system.*

resolution of 0.3 nm FWHM, which is not enough to resolve every single emission line. All spectra were analyzed by fitting 7 Gaussian shaped peaks to the data (see Table 7.2). The resulting photon yields were converted to emission cross sections by calibrating via known cross sections for He^{2+}+H_2O (Seredyuk et al., 2005a; Bodewits et al., 2006).

The observed emission lines provide two independent, direct measures of the TS ratios: the ratio between the triplet and singlet 3d–2p transitions, H_3, and the ratio between the triplet and singlet 4s,d–2p transitions, H_4:

$$H_3 = \frac{\sigma(\mathrm{3d})_T + \sigma(\mathrm{4f})_T}{\sigma(\mathrm{3d})_S + \sigma(\mathrm{4f})_S} \tag{7.6}$$

$$H_4 = \frac{\sigma_{em}(\mathrm{4s-2p})_T + \sigma_{em}(\mathrm{4d-2p})_T}{\sigma_{em}(\mathrm{4s-2p})_S + \sigma_{em}(\mathrm{4d-2p})_S} \tag{7.7}$$

To obtain the H_3 ratio, the $\sigma(\mathrm{3d})^*_T$ population cross section should be corrected for cascade

Table 7.2: *Fit results - measured emission cross sections for collisions between C^{5+} and H_2O, at different collision energies. All cross sections are in units of 10^{-16} cm^2. Only relative errors are given. The systematic uncertainty is approximately 25%.*

#	λ (nm)	Transitions	Coll. energy (keV/amu)		
			0.113	0.375	3.75
1	17.3	4p–2s (T)	1.0 ± 0.1	0.7 ± 0.1	1.1 ± 0.1
2	18.8	4d–2p (T), 4s–2p (T), 4p–2s (S)	6.1 ± 0.6	2.0 ± 0.2	2.0 ± 0.2
3	19.8	4d–2p (S), 4s–2p (S)	2.5 ± 0.2	0.7 ± 0.1	0.8 ± 0.1
4	22.7	3p–2s (T)	14 ± 1.4	7.2 ± 0.7	4.4 ± 0.4
5	24.8	3d–2p (T), 3p–2s (S)	2.7 ± 0.3	4.0 ± 0.4	10 ± 1.0
6	26.0	3s–2p (T,S)	2.6 ± 0.3	1.9 ± 0.2	1.8 ± 0.2
7	26.7	3d–2p (S)	2.1 ± 0.2	2.4 ± 0.2	3.6 ± 0.4

population from the 4p-state in the triplet system, because this 4p-2s cascade transition is negligible in the singlet system:

$$\sigma(3d)^*_T = \sigma_{em}(3d-2p)_T - 0.04\sigma_{em}(4p-2s)_T \tag{7.8}$$

The observed emission lines also allow us to deduce emission cross sections for the K-series, observable in X-ray. To do this, we first assume that singlet np–2s transitions do not contribute significantly to the observed emission features, because these transitions have very small branching ratios compared to transitions directly to the ground state (less than 0.06 for $n = 3,4$). Close inspection of the measured spectra (Fig. 7.2) shows that there is no detectable 1s5p-1s2s line emission around 15.6 nm. It is therefore save to assume that contributions from capture into the $n = 5$ states are negligible. A third assumption is that the $n\ell$-distribution is equal in the triplet and singlet systems.

Kα line emission cross sections can then be estimated from the cascade population cross sections of the 1s2p($^3P_{1,2}$) and 1s2s($^3S_1$) states by using apparent branching ratios from Table 7.1

$$\sigma_{em}(x+y) = 0.11\sigma(2p)^*_T \tag{7.9}$$

$$\sigma_{em}(z) = \sigma(2s)^*_T \tag{7.10}$$

where the cascade population cross sections can be deduced from the measured emission cross sections:

$$\sigma(2s)^*_T = \sigma_{em}(4p-2s)_T + \sigma_{em}(3p-2s)_T + 0.89\sigma(2p)^*_T \tag{7.11}$$

$$\begin{aligned}\sigma(2p)^*_T = {} & \sigma_{em}(4s,d-2p)_T + \sigma_{em}(3d-2p)_T \\ & + 0.32\sigma_{em}(4p-2s)_T + \frac{H_3}{H_3+1}\sigma_{em}(3s-2p)_{ST}\end{aligned} \tag{7.12}$$

In a similar manner, the emission cross section of the resonance line is found from the population of the 1s2p($^1P_1$) state:

$$\sigma_{em}(w) = \sigma_{em}(4s,d-2p)_S + \sigma_{em}(3d-2p)_S + \frac{1}{H_3+1}\sigma_{em}(3s-2p)_{ST} \tag{7.13}$$

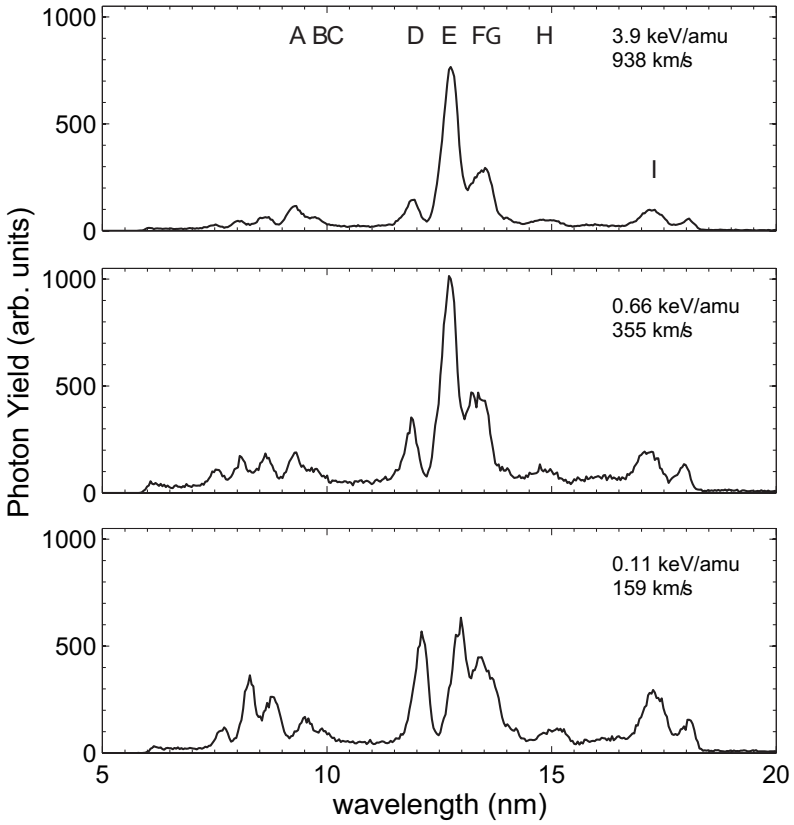

Figure 7.3: *Charge exchange spectra for collisions between O^{7+} and H_2O, at different velocities. The spectra are all on the same scale, i.e. corrected for the inlet pressure and integration time. The labels A-I refer to Table 7.3.*

With our spectrometer, the K-series cannot be observed directly. Emission cross sections for Kβ and Kγ lines can be estimated by weighting the triplet populations with the triplet-singlet ratio and the relevant branching ratios:

$$\sigma_{em}(3\mathrm{p}-1\mathrm{s})_S = \frac{1}{H_3}\cdot\sigma_{em}(3\mathrm{p}-2\mathrm{s})_T \tag{7.14}$$

$$\sigma_{em}(4\mathrm{p}-1\mathrm{s})_S = \frac{0.95}{0.76}\frac{1}{H_4}\cdot\sigma_{em}(4\mathrm{p}-2\mathrm{s})_T \tag{7.15}$$

Finally, total one electron capture cross sections can be estimated by:

$$\sigma_t = \sigma_{em}(w)+\sigma_{em}(x,y)+\sigma_{em}(z)+1.05\sigma_{em}(3\mathrm{p}-1\mathrm{s})_S+1.05\sigma_{em}(4\mathrm{p}-1\mathrm{s})_S \tag{7.16}$$

7.2.2 O^{7+}

The analysis of OVII spectra due to single electron capture by O^{7+} from H_2O molecules is even more complex than the CV spectra. More emission lines are present due to the fact that the higher charge state of the oxygen ion leads to population of the $n = 5,6$ shells. Typical spectra for charge exchange between H-like oxygen and H_2O are shown in Fig. 7.3. The data were analyzed by fitting 9 Gaussians to the spectra, see Table 7.5.

The spectra provide one independent measures J_3 of the TS ratio following one-electron capture:

$$J_3 = \frac{\sigma_{em}(3\mathrm{d}-2\mathrm{p})_T - 0.04\sigma_{em}(4\mathrm{p}-2\mathrm{s})}{\sigma_{em}(3\mathrm{d}-2\mathrm{p})_S} \tag{7.17}$$

In the singlet system, the 1s4p(^{1}P) state mainly relaxes directly to the ground state, whereas in the triplet system, a minor fraction cascades to the 1s3d(^{3}S) state. We therefore correct J_3 for this contribution by weighting the emission cross section of the 4p–2s(T) with the relevant branching ratio.

From these relations, the following emission cross sections can be derived for the K-series:

$$\sigma_{em}(\mathrm{K}\gamma) = \frac{0.93}{0.75}\frac{1}{J_3}\sigma_{em}(4\mathrm{p}-2\mathrm{s})_T \tag{7.18}$$

$$\sigma_{em}(\mathrm{K}\beta) = 0.95\frac{1}{J_3}\sigma_{em}(3\mathrm{p}-2\mathrm{s})_T \tag{7.19}$$

7.2.3 Uncertainties

The results are subject to a number of uncertainties. The dominating absolute uncertainty is that arising from the spectrometer's calibration by means of cross sections for CXE from He^{2+} ions, and is approximately 20% (Bodewits et al., 2006). This error affects all data points, and leads to a simple scaling factor. A more complex error is due to the uncertainty in the wavelength dependent sensitivity of the spectrometer, which we estimate to be 10 – 15%. Added in quadrature these uncertainties lead to an absolute systematic uncertainty of 25%. The uncertainty associated with the wavelength-dependent sensitivity may also influence the relative line strengths which are of importance when assessing cascade contributions. Target fluctuations were controlled by performing regular calibration measurements, but lead to a random error in the order of 5%. Statistical errors for these experiments were small due to high photon yields and never exceeded 1% (1σ). Therefore we assume a relative uncertainty of 10% in the line emission cross sections.

Table 7.3: *Fit results - measured emission cross sections for collisions between O^{7+} and H_2O, at different collision energies. All cross sections are in units of 10^{-16} cm^2. Only relative errors are given. The systematic uncertainty is approximately 25%.*

#	λ (nm)	Line(s)	Collision Energy (keV/amu)							
			0.13	0.22	0.66	1.3	2.6	3.3	3.9	4.6
A	9.1	4p–2s (T)	0.9 ± 0.1	0.8 ± 0.1	0.8 ± 0.1	0.9 ± 0.1	0.4 ± 0.1	0.7 ± 0.08	0.9 ± 0.09	0.9 ± 0.1
B	9.7	4s,d–2p (T), 4p–2s (S)	3.7 ± 0.4	3.4 ± 0.4	3.8 ± 0.4	3.4 ± 0.3	4.3 ± 0.4	3.2 ± 0.3	3.0 ± 0.3	3.0 ± 0.3
C	10.0	4s,d–2p (S)	1.7 ± 0.2	1.8 ± 0.2	1.6 ± 0.2	1.5 ± 0.2	1.7 ± 0.2	1.2 ± 0.1	1.2 ± 0.1	1.1 ± 0.1
D	12.0	3p–2s (T)	7.6 ± 0.8	6.8 ± 0.7	4.1 ± 0.4	2.8 ± 0.3	2.9 ± 0.3	2.1 ± 0.2	2.0 ± 0.2	2.1 ± 0.2
E	12.8	3d–2p (T), 3p–2s (S) .	7.6 ± 0.8	10 ± 1.0	13 ± 1.3	12 ± 1.2	15 ± 1.5	10 ± 1.0	9.8 ± 1.0	11 ± 1.1
F	13.3	3s–2p (T)	5.1 ± 0.5	5.3 ± 0.5	5.0 ± 0.5	3.8 ± 0.4	3.9 ± 0.4	3.1 ± 0.3	2.8 ± 0.3	2.8 ± 0.3
G	13.7	3s,d–2p (S)	3.3 ± 0.3	3.8 ± 0.4	4.3 ± 0.4	3.9 ± 0.4	4.4 ± 0.4	3.2 ± 0.3	3.2 ± 0.3	3.2 ± 0.3
H	15.0	OVI	0.7 ± 0.07	0.7 ± 0.08	0.6 ± 0.1	0.0 ± 0.00	0.5 ± 0.05	0.3 ± 0.03	0.4 ± 0.04	0.3 ± 0.03
I	17.3	OVI	3.0 ± 0.3	2.9 ± 0.3	1.6 ± 0.2	0.0 ± 0.0	1.5 ± 0.2	1.0 ± 0.10	0.8 ± 0.08	0.9 ± 0.1

7.3 Results and Discussion

7.3.1 Triplet-Singlet Ratios

The measured velocity dependence of the accessible CXE triplet to singlet ratios is shown in Fig. 7.4. Our measurements show that in collisions between H-like carbon and oxygen with water, singlet and triplet states are populated statistically at high velocities. At low collision velocities, all TS ratios are significantly lower than 3. In particular the CV H_3 ratio decreases quickly with decreasing velocity, and this effect should be observable at normal slow solar wind interactions (300km s^{-1} or 0.5 keV/amu).

Unfortunately, there exists no simple model to describe TS ratios. Parallel to the distribution over the l-shells, it is to expected that at low velocities, capture cross sections become more and more dependent on the exact nature of the state (binding energies, angular momentum). Qualitatively we find a statistical distribution at high velocities, whereas at low velocities, all measured TS ratios decrease significantly below 3.

7.3.2 Partial Cross Sections

C^{5+} – The result of our spectral analysis are shown in Tables 7.4 and 7.5 for C^{5+} and O^{7+}, respectively. The EUV CXE spectra of CV allow for the derivation of emission cross sections of all the lines detectable in X-ray (i.e. the K-series, the forbidden line and the intercombination line). The Classical Over-the-Barrier model shows that capture into $n = 4$ is nearly resonant (Fig. 7.5).

In Fig. 7.7 our results are compared with theoretical state selective, velocity dependent cross sections for collisions of bare ions with atomic hydrogen (Errea et al., 2004; Fritsch and Lin, 1984; Green et al., 1982; Shipsey et al., 1983), see Chapter 8. At high velocities, the results for C^{5+} are in good agreement with the theoretical cross sections, but at lower velocities the theoretical cross sections underestimate the emission cross sections. At velocities typical for the slow solar wind (300 km s^{-1}), the most important features (i.e. the CV w, x, y and z lines) are underestimated by a factor of approximately 1.5. The Kβ might be underestimated more, but is only a minor contributor to emission in astrophysical environments.

O^{7+} – The OVII spectrum contains too many unresolved lines to allow for an analysis comparable to that of the C^{5+} data. In particular, the spectral resolution of our experiment is not sufficient to resolve all the $n = 5$ and $n = 6$ lines that are present below 9 nm. Nevertheless, some general trends can be observed. From the Classical Over-the-Barrier model, it is to be expected that capture into $n = 5$ is the dominant reaction channel (Fig. 7.5). Hasan et al. (2001) measured the n-distribution at 2 keV/amu and observed indeed that most capture occurs into $n = 5$ (85%), and capture into n=4 and n=6 contribute 14% and 1.4%, respectively.

Emission cross sections of the Kβ and Kγ lines were derived from the spectra. Compared to theory for bare nitrogen ions colliding on H (Fig. 7.7), the presented emission cross sections are roughly a factor of 2 smaller. Greenwood et al. (2001) directly measured emission cross sections for $O^7+ + H_2O$ with an X-ray spectrometer. For a collision energy of 2.7 keV/amu, they found much larger emission cross sections of (3.0 ± 0.4) and

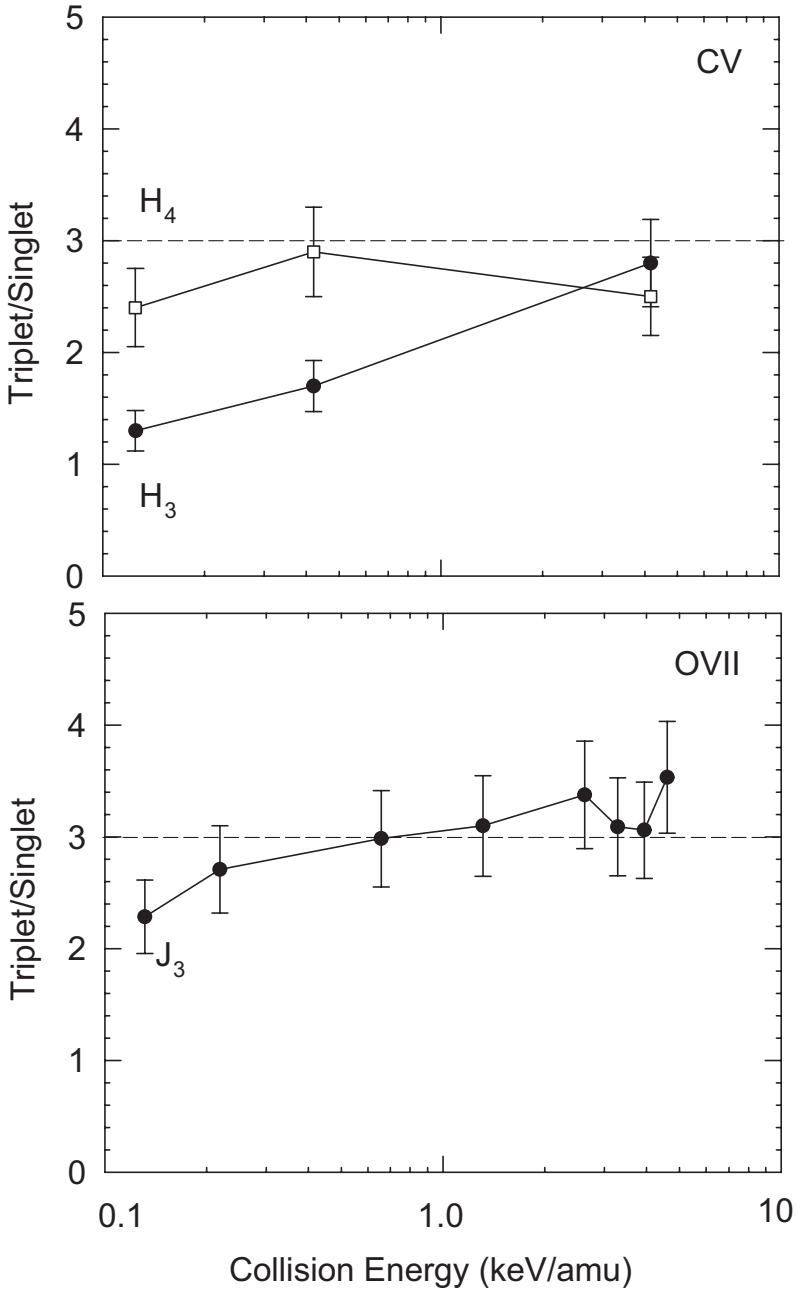

Figure 7.4: *Triplet to singlet ratios for charge exchange between C^{5+} and H_2O (upper panel) and O^{7+} and H_2O (lower panel) for different collision energies. Lines are drawn to guide the eye. The dashed line indicates the statistical triplet to singlet ratio (3).*

Table 7.4: *Triplet-singlet ratios, emission cross sections and total one electron capture cross sections for collisions between C^{5+} and H_2O, at different collision energies. All cross sections are in units of 10^{-16} cm^2. Only relative errors are given. The systematic uncertainty is approximately 25%.*

Coll. energy (keV/amu) Velocity (km s^{-1})	0.113 170	0.375 309	3.75 979
H_3	1.3 ± 0.2	1.7 ± 0.2	2.8 ± 0.4
H_4	2.4 ± 0.4	2.9 ± 0.4	2.5 ± 0.4
x+y	1.2 ± 0.08	0.8 ± 0.05	1.5 ± 0.1
z	24 ± 1.5	14 ± 0.9	18 ± 1.0
w	5.8 ± 0.4	3.8 ± 0.3	4.9 ± 0.4
Kβ	11 ± 1.9	4.4 ± 0.8	1.6 ± 0.3
Kγ	0.5 ± 0.1	0.3 ± 0.04	0.6 ± 0.1
Total	43 ± 2.6	24 ± 1.2	26 ± 1.2

$(3.5 \pm 0.6) \times 10^{-16}$ cm^2 for the Kβ and Kγ, respectively.

7.3.3 Total Cross Sections

Total charge changing cross sections for C^{5+}+H_2O collisions have recently been measured by Mawhorter et al. (2007). They measured a charge changing cross section of $(42 \pm 3.2) \times 10^{-16}$ cm^2. This is much larger than the one electron capture cross sections measured by us at comparable energies, which by interpolation would be $(25 \pm 6.6) \times 10^{-16}$ cm^2. This difference can only be attributed to auto-ionizing double electron capture (A2C) processes. Such processes most likely populate either the ground state or the first excited state of CV, as A2C -enhanced population of the $n = 3$ state would have been directly observable in our PES experiments. For two electron charge transfer, Mawhorter et al. (2007) measured a cross section of $(6.0 \pm 1.0) \times 10^{-16}$ cm^2. According to our interpretation, the auto-ionizing double electron capture cross section would be approximately $(17 \pm 7.3) \times 10^{-16}$ cm^2, or roughly a factor of 3 larger than the cross section for bound double electron capture. As in the case of O^{6+} + H_2O collisions (see Chapter 6) the cross section for twofold charge

Table 7.5: *Triplet-singlet ratios, emission cross sections and total one electron capture cross sections for collisions between O^{7+} and H_2O, at different collision energies. All cross sections are in units of 10^{-16} cm^2. Only relative errors are given. The systematic uncertainty is approximately 25%.*

E (keV/amu) v (km s^{-1})	0.13 159	0.22 205	0.66 355	1.3 501	2.6 709	3.3 793	3.9 868	4.6 938
J_3	2.3 ± 0.3	2.7 ± 0.4	3.0 ± 0.4	3.1 ± 0.4	3.4 ± 0.5	3.1 ± 0.4	3.1 ± 0.4	3.5 ± 0.5
Kγ	0.5 ± 0.1	0.4 ± 0.1	0.3 ± 0.1	0.4 ± 0.1	0.2 ± 0.03	0.3 ± 0.1	0.4 ± 0.1	0.3 ± 0.1
Kβ	3.2 ± 0.6	2.4 ± 0.5	1.3 ± 0.3	0.8 ± 0.2	0.8 ± 0.2	0.7 ± 0.2	0.6 ± 0.2	0.6 ± 0.2

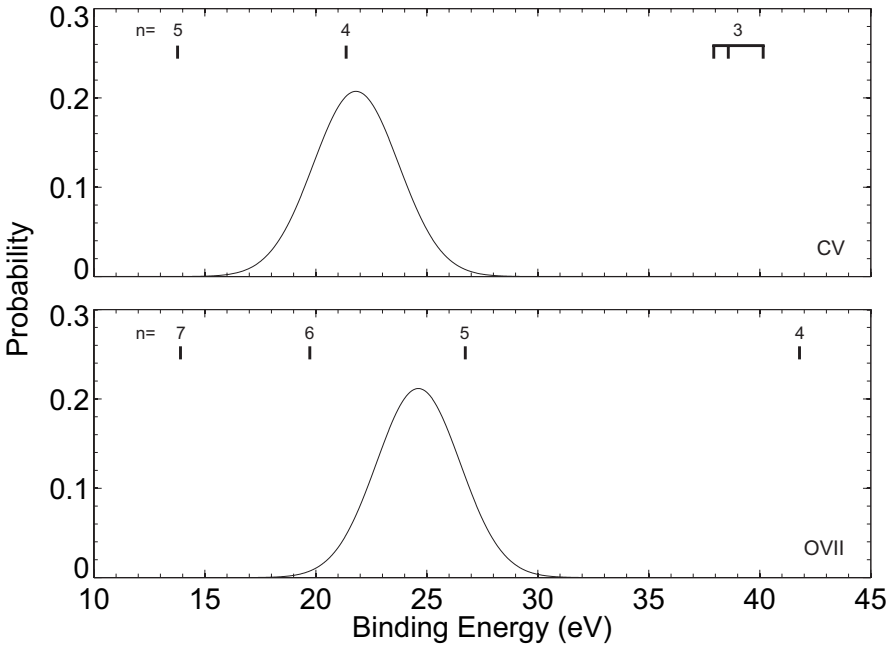

Figure 7.5: *Classical Over-the-Barrier reaction windows for single electron capture by C^{5+} (top panel) and O^{7+} (lower panel) from H_2O.*

transfer measured by Mawhorter et al. (2007) is most likely due to 3 (or more) electron transfer.

Our experiment ensures single collision conditions, and the OVI emission detected allow for an estimate of double electron capture cross sections. The spectra show the presence of OVI $1s^2 3p–1s^2 2s$ (15.0 nm) and $1s^2 3d–1s^2 2p$ (17.3 nm) emission lines. The emission cross sections of both lines decrease with increasing collision velocity. Adding the two emission cross sections together, we find the minimum cross section for bound double electron capture to decrease from $(3.7 \pm 1.0) \times 10^{-16}$ cm^2 at 0.13 keV/amu to $(1.2 \pm 0.3) \times 10^{-16}$ cm^2 at 4.6 keV/amu.

It is interesting to compare these results with Over-the-Barrier predictions and charge changing measurements. Greenwood et al. (2001) measured one, two- and threefold charge changing cross sections of $\sigma_{q,q-1} = (53 \pm 1) \times 10^{-16}$ $\sigma_{q,q-2} = (8 \pm 1) \times 10^{-16}$ and $\sigma_{q,q-3} < 3 \times 10^{-16}$ at collision energies of 2.72 keV/amu. Our lower limit for bound double capture cross sections is about 40% smaller than the double charge changing cross section of Greenwood et al. (2001). These results seem consistent with ours, in particular given that we observed only the strongest OVI emission lines.

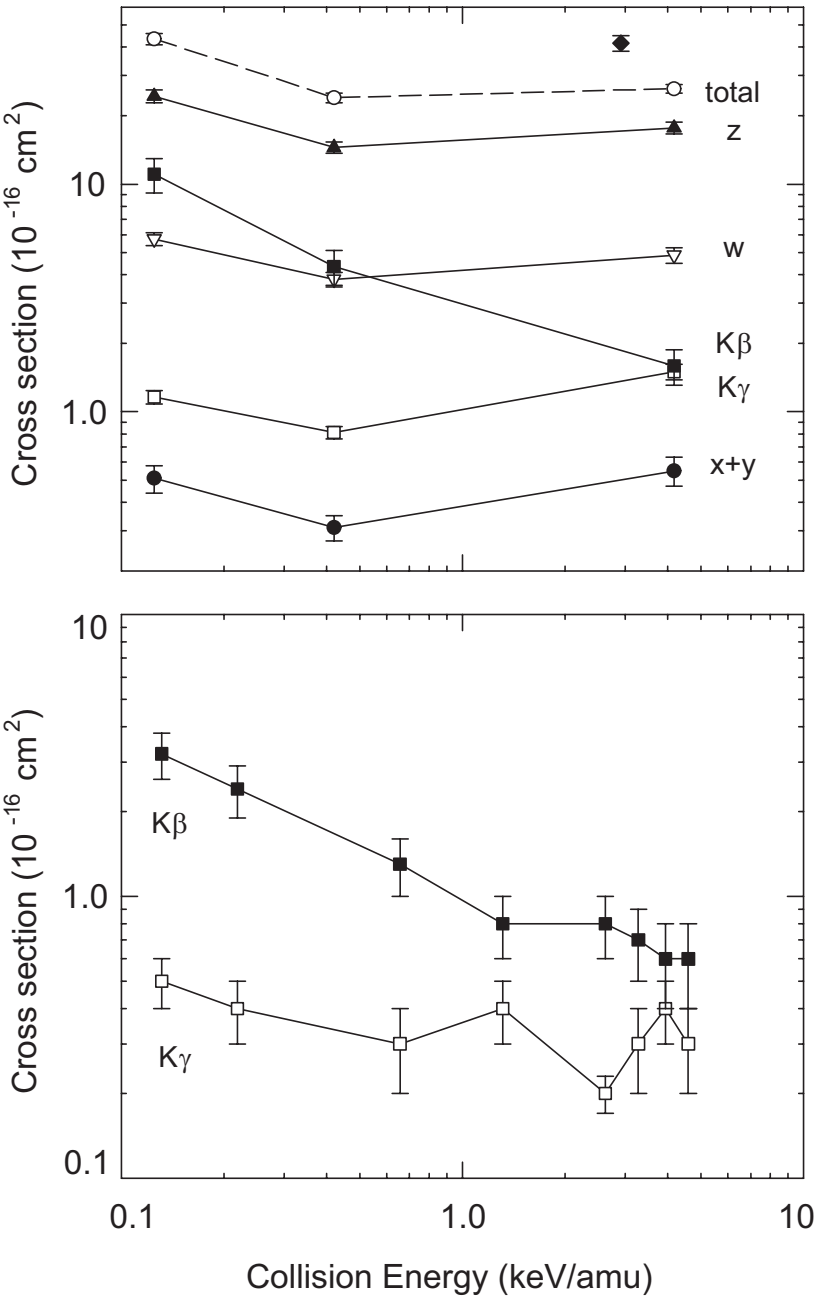

Figure 7.6: *Velocity dependence of X-ray emission cross sections.* ***Top panel:*** C^{5+} + H_2O. *Indicated are* ▲ *– z;* ▽ *– w;* □ *– x + y;* ■ *– Kβ;* ● *–Kγ and the total one electron capture cross section* ○ *–*σ_t*;* ♦ *– total charge changing cross section (Mawhorter et al., 2007).* ***Lower panel:*** O^{7+} + H_2O. *Indicated are:* ■ *– Kβ;* ● *–Kγ. Lines are drawn to guide the eye, and only relative errors are given. The systematic uncertainty is approximately 25%.*

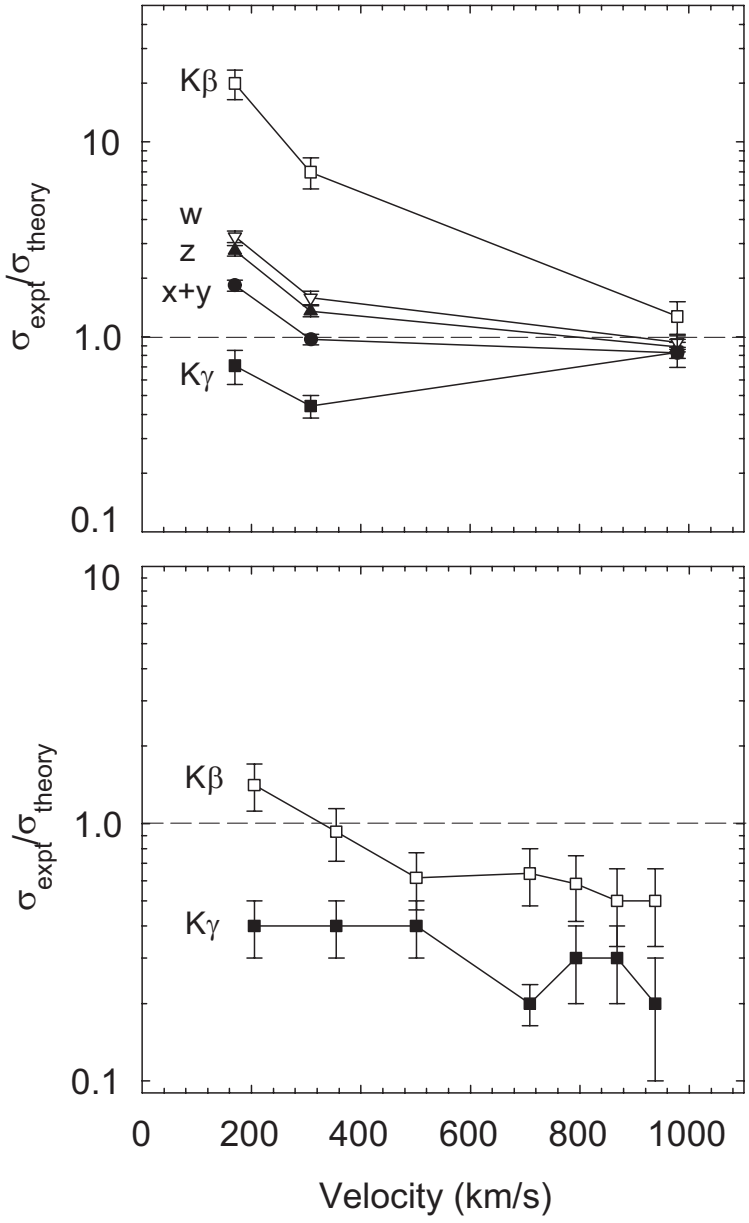

Figure 7.7: *Ratio between experimentally obtained cross sections and theoretical cross sections for bare ions colliding on H, see text.* ***Top panel:*** *C^{5+} + H_2O. Indicated are ▲ − z; ▽ − w; □ − x + y; ■ − Kβ; ● − Kγ.* ***Lower panel:*** *O^{7+} + H_2O. Indicated are: ■ − Kβ and ● − Kγ. Lines are drawn to guide the eye, and only relative errors are given. The systematic uncertainty is approximately 25%.*

Table 7.6: *Ionization potentials and resulting Over-the-Barrier predictions for capture distances and geometrical cross sections.*

#	IP_n (eV)	C^{5+}		O^{7+}	
		$R_{c,n}$ (a.u.)	σ_n (Å^2)	$R_{c,n}$ (a.u.)	σ_n (Å^2)
1	12.6	11.8	33	13.6	45
2	27	8.0	9	9.1	12
3	~45	6.5	19	7.4	24

7.4 Conclusions

Cometary X-ray spectra are dominated by the forbidden lines of H-like C and O following charge exchange with water and its dissociation products. The relative strength of these lines are determined by the distribution over triplet and singlet states into which the electrons are captured. We performed experimental studies of O^{7+} and C^{5+} colliding on water vapor and for the first time measured triplet-singlet population ratios. At high collision velocities, both the OVII and CV states are populated statistically. At lower velocities however, the ratios decrease significantly below 3. This effect is the strongest for CV, and this might be directly observable in interactions between comets and the slow solar wind.

From comparison with existing measurements, our results also allowed for a reconstruction of the relevant electron capture channels. Our findings are consistent with earlier experiments (Chapter 6) and show once again that auto-ionizing processes play an important role in charge transfer reactions.